Neutron-rich isotopes $^{54-57}$Ti

T. Dörfler, W.-D. Schmidt-Ott, and T. Hild
II. Physikalisches Institut, Universität Göttingen, D-37073 Göttingen, Germany

T. Mehren, W. Böhmer, P. Möller,* B. Pfeiffer, T. Rauscher,† and K.-L. Kratz
Institut für Kernchemie, Universität Mainz, D-55099 Mainz, Germany

O. Sorlin, V. Borrel, S. Grévy, D. Guillemaud-Mueller, A. C. Mueller, and F. Pougheon
Institut de Physique Nucléaire, CNRS-IN2P3, 91406 Orsay Cedex, France

R. Anne, M. Lewitowicz, A. Ostrowsky, M. Robinson, and M. G. Saint-Laurent
GANIL, BP 5027, 14021 Caen Cedex, France

(Received 2 November 1995)

The neutron-rich isotopes $^{54-57}$Ti and $^{58-60}$Cr are produced by fragmentation of a 64.5 MeV/nucleon $^{65}Cu^{26+}$ beam in a 90 mg/cm^2 ^{9}Be target. Following particle identification by energy loss and time of flight, the radioactive decay was observed by β singles and $\beta\gamma$-coincidence measurements. The results obtained for $^{58-60}$Cr are compared to previous results, whereas the decay of the $^{54-57}$Ti isotopes is studied here. γ-ray intensities and energies are estimated. The new experimental results are compared to quasi-random-phase-approximation predictions. [S0556-2813(96)00212-9]

PACS number(s): 27.40.+z, 27.50.+e, 23.40.−s, 25.70.Mn

I. INTRODUCTION

Intermediate-energy heavy-ion fragmentation has proven to be a promising and successful mechanism for the production of new exotic nuclei which often cannot be achieved by means of fission or compound nucleus reactions [1,2]. Investigations of isotopes with masses $40<A<80$ located between stability and neutron-drip line are of special interest since the surplus of neutrons is responsible for varying deformation exhibiting sensitive effects on the half-lives of these nuclei [3,4].

The isotopes $^{54-57}$Ti with neutron numbers $32\leqslant N\leqslant 35$ were investigated. As in the cases of calcium [5,6] and chromium [7,8], we expected a similarly striking decrease of half-lives when proceeding from the 32nd to the 33rd neutron. On the other hand, the situation in titanium could be similar to the one of neutron-rich sulphur and chlorine isotopes with closed neutron shell $N=28$. An effect of decreasing shell strength and the onset of collectivity were observed for ^{44}S [9].

Our results may be of relevance to the nucleosynthesis origin of correlated Ca-Ti-Cr-Fe FUN (fraction and unknown nuclear effects) anomalies in certain meteoric inclusions. For a recent survey on the identification of such isotopic anomalies see, e.g., Ref. [10]. Theoretical attempts to explain the occurence of the exotic abundances, including possible astrophysical scenarios as well as nuclear-physics clues, can be found in Refs. [11–15].

II. EXPERIMENTAL SETUP

A. Production, separation, and identification

In this experiment enriched ^{65}Cu has been used as a projectile at GANIL. Indeed, from its position in the chart of nuclei, projectilelike fragmentation of this nucleus should be well suited for the production of neutron-rich isotopes with masses $50\leqslant A\leqslant 60$. For the experiment, the intense primary 64.5 MeV/nucleon $^{65}Cu^{26+}$ beam of $\sim$300 e nA onto a 90 mg/cm^2 ^{9}Be target was used. The fragments were separated with the doubly achromatic LISE3 spectrometer [16,17] (see Fig. 1). The target was mounted at the entrance of the LISE3 spectrometer, and beryllium was chosen to optimize the production of fully stripped ions.

In a first attempt, the magnetic spectrometer was operated without any additional degrader in the intermediate focal plane. Ions having the same Av/Q ratio were analyzed by the dipoles 1 and 2 at the same magnetic rigidities. Here,

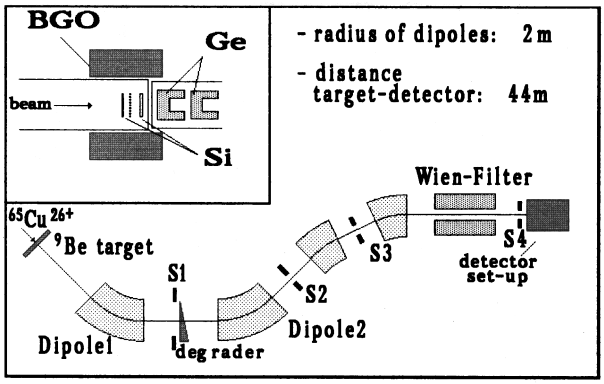

FIG. 1. Schematic view of the LISE3 spectrometer with the Wien filter. Inset: detection system consisting of three Si detectors, a BGO ring, and a Ge detector.

*Present address: P. Möller Scientific Computing and Graphics, Inc., Los Alamos, NM 87545.

†Present address: Institut für Theoretische Physik, Universität Basel, CH-4056 Basel, Switzerland.

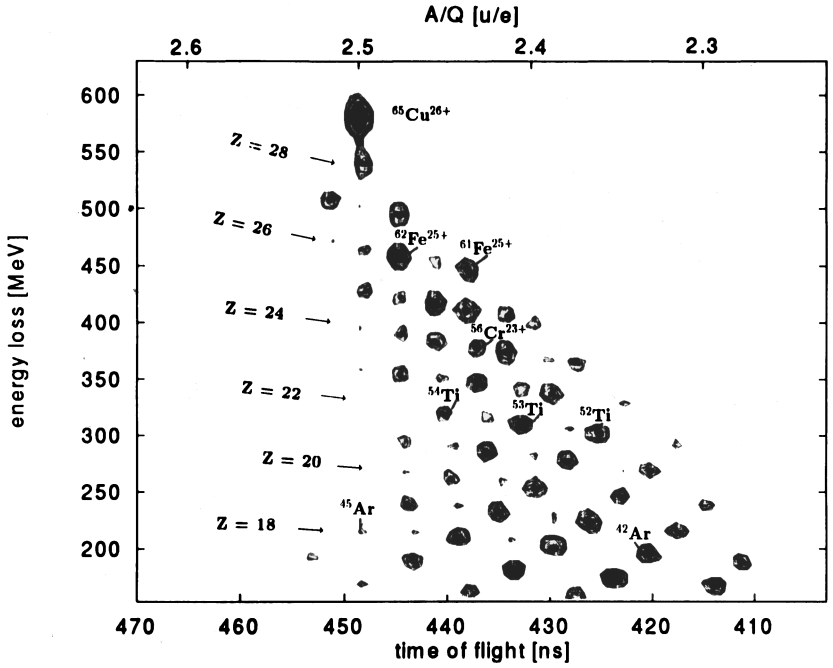

FIG. 2. Energy loss vs time of flight of fragments passing the spectrometer without an intermediate degrader. The spot of the primary $^{65}Cu^{26+}$ beam is clearly visible. With two other lower-Z isotopes—here ^{45}Ar and ^{42}Ar—all the other nuclei were identified. Some significant Z values are indicated. The time of flight is converted into A/Q values. For higher-Z, the main intensity is due to hydrogenlike fragments, for example $^{61,62}Fe^{25+}$ and $^{56}Cr^{23+}$; fully stripped ions prevail at lower-Z values.

Q denotes the charge state, v the velocity of the fragments after leaving the target, which roughly corresponds to the primary beam velocity, and A the mass of a fragment. The identification was performed by means of time-of-flight and energy loss analysis.

The fragments were implanted into a three-member Si telescope. The time of flight was given by the time interval between the energy loss signal ΔE of the heavy ion, measured in the first 300-μm Si detector, and the radio-frequency signal of the cyclotron. An energy loss vs time-of-flight plot is shown in Fig. 2. Subsequently, a calibration of the fragment identification according to the element number Z and the A/Q value was given from the position of the not completely stripped primary $^{65}Cu^{26+}$ beam. For identification of the charge state, an additional measurement of the residual energy of the fragment in the implantation detector was necessary.

The nuclei were implanted in a 500-μm Si(Li) detector, consisting of 12 adjacent horizontal strips. Each strip ($24\times2\times0.5$ mm) was operated with two amplifier chains, one for high-energy (heavy ions), and one for low-energy (β particles) signals. A third 3000-μm Si(Li) detector was used as a heavy-ion veto and β detector.

In a second setting of the spectrometer, the variety of detected fragments was reduced using a 221.5(10)-μm aluminum degrader in the intermediate focal plane. Thereby, an energy loss approximately scaling with A^3/Z^2 was introduced. The degrader thickness was inferred by analyzing the energy loss of several charge states of the primary beam passing the degrader. The second dipole was then set to a magnetic rigidity corresponding to the residual velocity of the desired fully stripped nucleus (see Table I). Only a few other isotopes also reached the final focus as shown in Fig. 3. In the two latter settings of Table I—corresponding to higher fragment velocities—an additional 200-μm Al foil was mounted between the first and the second Si detector to make sure that the fragments were stopped in the strip detector.

Figure 3 shows the energy loss of the fragments as function of the time of flight for one of the $B\rho$ settings. Similar displays were obtained in the two other runs with different $B\rho$ values (see Table I). For each run, the time of flight was

TABLE I. Experimental parameters used for the measurement of Ti and Cr isotopes; t_p is the time of β counting during which the beam was switched off. T_{tot} is the total length of the measurement. For each A/Q value, we have optimized the transmission of one isotope.

A/Q (u/e)	Optimized isotope	$(B\rho)_1$ (Tm)	$(B\rho)_2$ (Tm)	t_p (s)	T_{tot} (h)
2.48	^{57}V	2.7060	2.5800	2.0/3.3	3.2/10.3
2.52	^{53}Sc	2.7652	2.6511	3.3	10.0
2.57	^{54}Sc	2.8190	2.7052	1.6/3.3	20.2/2.3

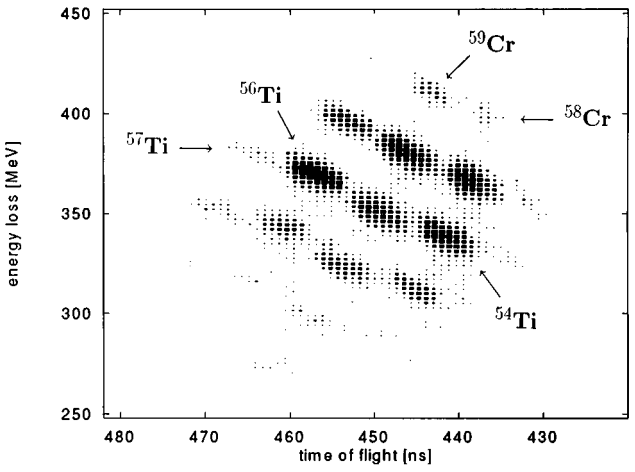

FIG. 3. Energy loss vs time of flight of investigated nuclei. The LISE3 spectrometer with a degrader in the intermediate focal plane was optimized for $A/Q=2.52$ (see Table I). Titanium and chromium isotopes are marked.

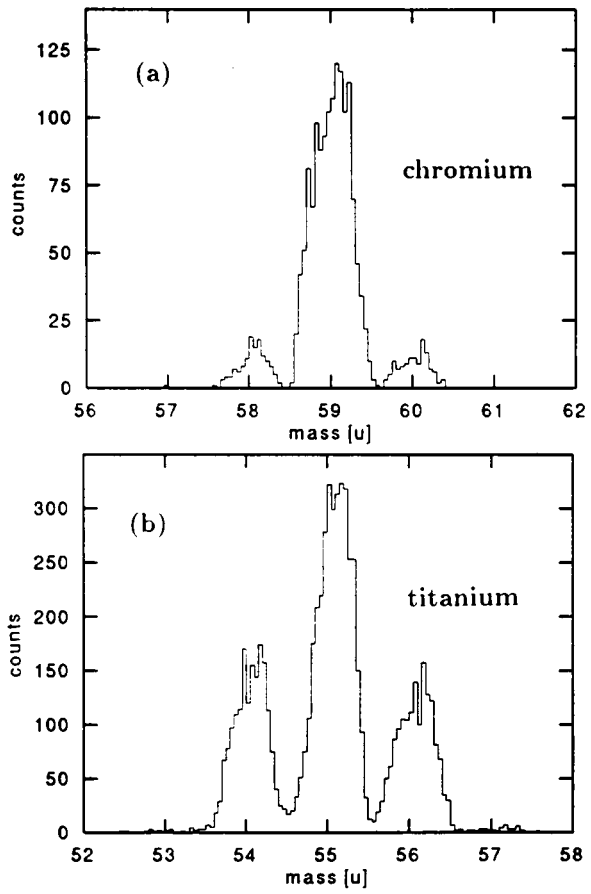

FIG. 4. Mass distributions comprising the total counting statistics of (a) chromium and (b) titanium isotopes. Safe limits were used to separate the isotopes from each other.

converted into mass number A of the chromium and of the titanium isotopes. The sum of the mass distributions of chromium and titanium isotopes under investigation are given in Fig. 4.

B. Beta and gamma-ray detection

The detector system is depicted in Fig. 1. The three Si detectors were used for fragment detection and identification. The second detector, having 12 strips, and the third one were also used for measuring β particles emitted from the implants. Electron detection was achieved starting 10 ms after the (more than 1000 times larger) heavy-ion energy signals for time intervals of t_p=1.6, 2.0, or 3.3 s (see Table I). Due to the detector geometry and the small energy loss of the electrons in the detectors, an average detection efficiency of 26(1)% was obtained. This applies for the β detection of nuclei with Q_β values between 4 and 10 MeV.

The Si detectors were surrounded by eight $Bi_4Ge_3O_{12}$ (BGO) crystals in a nearly 4π geometry. As compared to this BGO ring, the detection efficiency of the double-crystal Ge detector was small (see inset of Fig. 1). β-delayed γ rays were measured by the eight separated BGO segments of the ring. In this arrangement, γ-ray summing can be neglected. The well-known efficiency values of the BGO ring [18–20] could not be reached, due to a threshold in the γ spectrum of about 200 keV which was necessary to suppress x rays caused by the Wien filter. In accordance with a calibration with standard sources (^{22}Na, ^{137}Cs), actual values of the full energy efficiency ϵ_p and of the total detection efficiency $\epsilon_{\rm tot}$ were derived to be 0.75(3) and 0.75(3) at 400 keV, 0.65(3) and 0.70(3) at 600 keV, 0.45(3) and 0.55(3) at 1 MeV, and 0.33(3) and 0.51(3) at 1.5 MeV.

In the energy range between 0.2 and 1.5 MeV, the averaged total γ-detection efficiency $\overline{\epsilon_{\rm tot}}$ was 66(4)%. Consequently, the $\beta\gamma$-coincidence efficiency was 17(1)%. Since the BGO detector resolution and gain are temperature dependent [20], the system was stabilized at 18 °C. For each of the BGO segments a FWHM resolution of 120 keV and 230 keV was obtained for 662-keV and 1275-keV γ radiation, respectively.

After implantation and identification of a fragment, the ^{65}Cu beam was switched off for the interval t_p adapted to the half-life of the β decay under investigation. The data acquisition of decay events was performed during this period. Each detector signal was tagged with the clocktime subdivided into 1-ms intervals by making use of two timing-scale modules. The increment of the scalers was 1 ms and 4096 ms. Prompt $\beta\gamma$ coincidences were measured with a time-to-amplitude converter using the β signals as start and the signal of any of the BGO segments as stop.

III. BACKGROUND DETERMINATION

As can be seen in Fig. 3, about 10 parent isotopes were detected for each $B\rho$ setting. Each implanted fragment was identified and its β decay measured. The background in each strip is caused by the decays of the daughter activities of the implants. During the experiment, a constant background rate is expected at a nearly stable beam current after a short interval in which the radioactive equilibrium has been established. Our background determination is based upon this assumption. Another small contribution may come from long-lived decay products of the implants of the many isotopes detected in the earlier calibration run (see Fig. 2).

After implantation and identification of a fragment three strips were chosen for β detection, namely the implantation strip plus the two neighboring β detectors. The other nine strips were used for background counting during this measuring period t_p. The next implantation may take place in another strip. Thus, the role of the strips to measure β particles and background may change with each implantation. During an experiment lasting several hours it was counted how often each strip detector was used for β ray (plus background) measurement, and for background counting only. In this way, for each strip the number of background events and their energy distribution was normalized. The background is larger for the strips positioned in the center of the beam spot than for those at the edges and roughly scales with the number of implants.

The third detector was also used for β counting. Its background was measured during the short beam-on periods of the ^{65}Cu beam, i.e., after the t_p counting periods and before the implantation of the next fragment. Here, the total time of the background measurement was normalized to the sum of the β counting periods.

The background of $\beta\gamma$ coincidences in Fig. 5 is measured correspondingly by registering the coincidence events be-

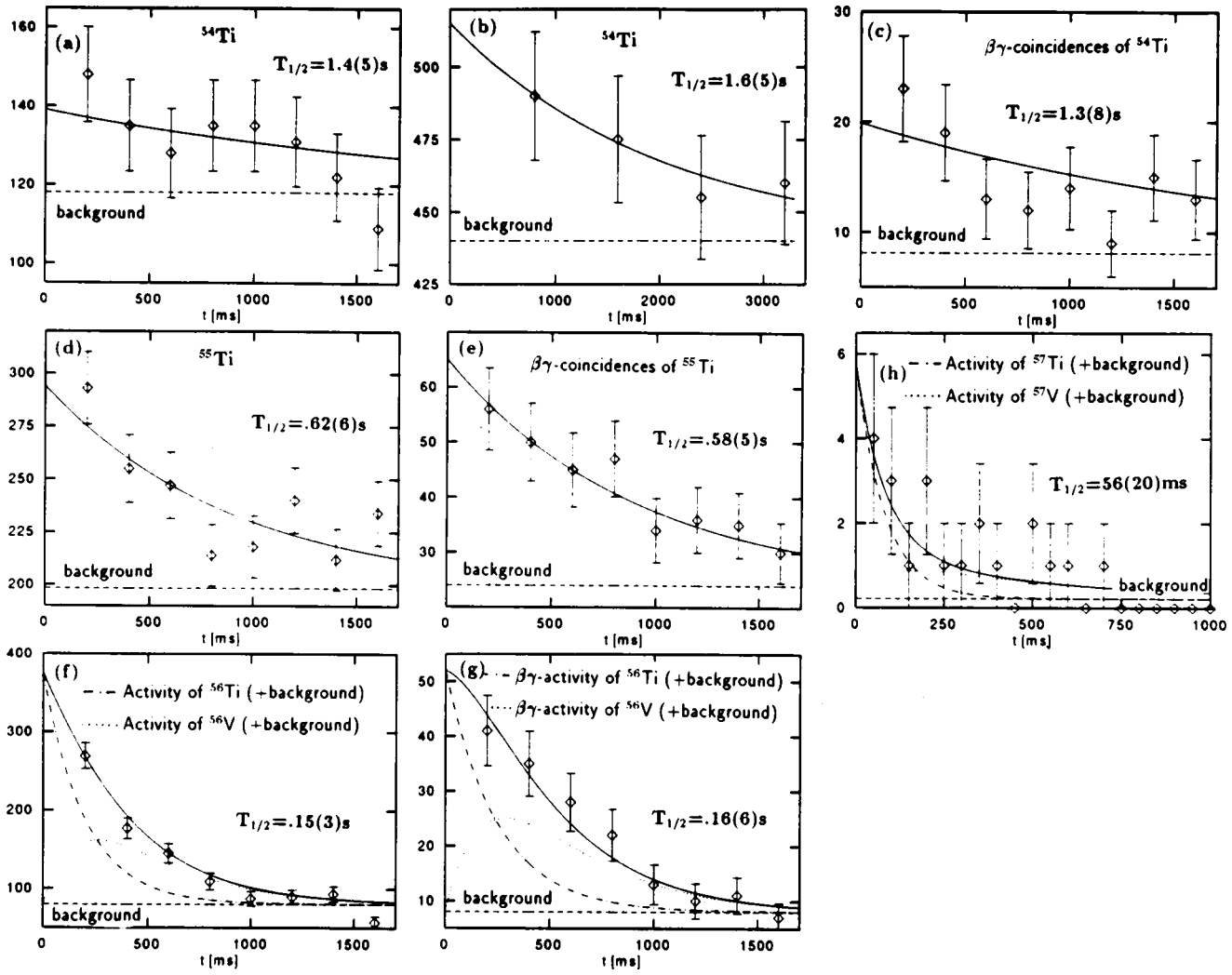

FIG. 5. Half-life spectra of $^{54-57}$Ti. The solid lines correspond to the data fits. The background is given by dashed lines and in the case of ^{56}Ti and ^{57}Ti the dotted lines mark the activities of the daughter nuclei on top of the background. The dash-dotted lines in (f)–(h) correspond to the decay of the implanted ^{56,57}Ti plus background. The data points of the spectra are plotted at the end of the integrating periods.

tween γ radiation and the background of the β detectors. Similarly, the energy distribution of the background as given in Fig. 6 was derived by gating the γ spectra with the β-ray background.

IV. HALF-LIFE AND γ-RAY MEASUREMENTS

The particle stability of neutron-rich titanium isotopes was demonstrated earlier [21,22]. The β half-lives and incipient structure measurements, however, are reported for the first time.

This half-life determination made use of the multistrip Si detector to measure both the fragments and the background decay. The decay curves are given in Fig. 5. The novel method was tested with previously known chromium isotopes and then applied to the measurement of unknown half-lives of neutron-rich isotopes. Our analysis made use of the Marquardt-Levenberg method [23] where the uncertainties of all the parameters are incorporated in the errors of the half-lives. The new half-life values are given in Table II.

All the γ-ray spectra were measured in coincidence with β radiation. The data points of Fig. 6 were fitted using the known BGO response function to monoenergetic γ rays, i.e., full energy and Compton peaks. For the decay of each isotope the feeding of excited states and of the ground state in the daughters was derived by comparing the total number of β-ray singles and of $\beta\gamma$ coincidences (Fig. 5). The relative feeding of the excited states was taken from the γ-ray spectra in Fig. 6. These data are contained in Table III.

A. The new isotopes $^{54-57}$Ti

For even-even ^{54}Ti, the half-life analysis was performed for β-ray singles in time intervals of t_p=1.6 [see Fig. 5(a)] and 3.3 s [see Fig. 5(b)], and for $\beta\gamma$ coincidences in the interval of 1.6 s [see Fig. 5(c)]. The results are in good agreement, and their mean value $T_{1/2}^{\text{expt}}$=1.5 (4) s is given in Table II. For this analysis the activity of the 49.8-s-^{54}V daughter [24] is negligible. The γ-ray spectrum given in Fig. 6(b) might indicate a γ line at $\approx$0.9 MeV and possibly some γ-ray strength below this energy. Within the experimental uncertainty no difference between the number of $\beta\gamma$ coinci-

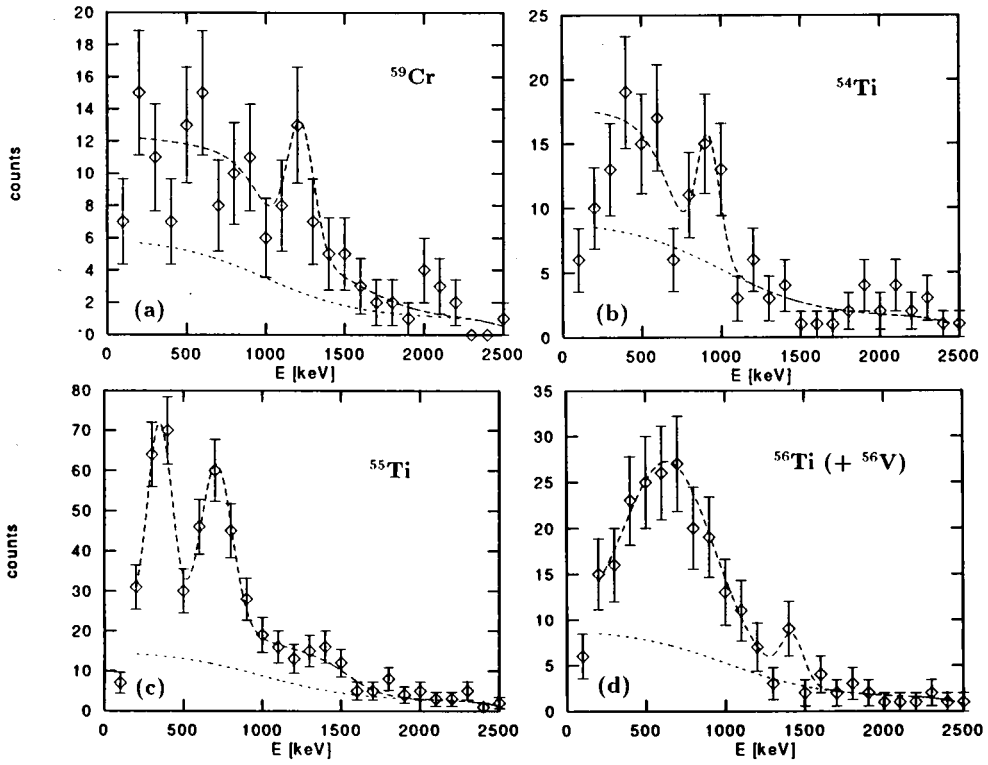

FIG. 6. BGO spectra of ^{59}Cr, ^{54}Ti, ^{55}Ti, and ^{56}Ti. For ^{59}Cr, after background subtraction the spectrum was fitted by the response function of the known 1239-keV γ line. In the case of ^{54}Ti, a 0.9-MeV γ line and a hump of unresolved radiation are outlined. In the ^{56}Ti spectrum, the γ-ray hump is caused by the ^{56}Ti and the ^{56}V daughter decay (see text). In the spectra the dashed lines represent the experimental background.

dences and β-ray singles was observed. The β intensity which is feeding states below 0.9 MeV is smaller than 30%. The β decay of the isotope ^{54}Ti might feed low-spin states in ^{54}V. Presumably for this reason we do not observe the γ rays of the in-beam reaction ^{48}Ca(^{9}Be, $2np\gamma$)^{54}*V [25].

For ^{55}Ti, the half-life results are given in Figs. 5(d) and 5(e). The measured values show good agreement, and the mean value $T_{1/2}^{\text{expt}}=0.60$ (4) s has been derived and is given in Table II. The comparison of the number of $\beta\gamma$ coincidences and β singles gave a ground-state–to–ground-state feeding of 60%. According to Fig. 6(c), the two γ rays of 0.3 and 0.7 MeV have similar intensities. In addition, the number of counts in each γ peak corresponds to the total number of $\beta\gamma$ coincidences [see Fig. 5(e)]. Consequently, the two γ rays very probably follow in cascade, as given in Table III. For the half-life measurements the grow-in of the ^{55}V daughter activity with $T_{1/2}=6.54$ s [26] could be neglected. Our ^{55}Ti half-life measurement can be compared with recent values from high-energy ^{86}Kr fragmentation studies which give a smaller value of 0.31 (4) s [27].

For the analysis of the ^{56}Ti half-life we took into account the growth and decay of the ^{56}V daughter. The latter decay has been measured recently with $T_{1/2}^{\text{expt}}(^{56}\text{V})=233$ (20) ms [28]. The decay curves are depicted in Figs. 5(f) and 5(g). The half-life $T_{1/2}^{\text{expt}}(^{56}\text{Ti})=0.15$ (3) s has been derived from the two measurements and is given in Table II. Adopting the recent result $T_{1/2}^{\text{expt}}(^{56}\text{V})=0.30$ (3) s of Ref. [27], the growth-and-decay analysis for ^{56}Ti has been repeated increasing the ^{56}Ti half-life to the value 0.17 (3) s, quite within the margins of our experimental error.

The γ spectrum in Fig. 6(d) shows unresolved intensity in a broad energy range. Using our results for the γ decay of ^{56}V [29], we estimated about half of the γ rays of Fig. 6d to belong to the ^{56}Ti parent, the other half to the ^{56}V daughter decay. Comparing the numbers of ^{56}Ti β singles and $\beta\gamma$-coincidence events it can be concluded that excited states in the region of 0.2–0.8 MeV are fed in about 40% of all β decays. As in ^{54}Ti β decay, a direct ground-state feeding can be excluded. Therefore, the residual β strength might feed low-lying excitation states in ^{56}V.

TABLE II. Comparison of experimental half-lives $T_{1/2}^{\text{expt}}$ and calculated values $T_{1/2}^{\text{th}}$. For each isotope two QRPA calculations were performed using the deformation ϵ_2^E derived from the ETFSI model for the parent nucleus and the deformation ϵ_2^F derived from the FRDM model for the daughter nucleus (see text). Experimental Q_β values were used.

Isotope	$T_{1/2}^{\text{expt}}$ (s)	Q_β (keV)	ϵ_2^E	$T_{1/2}^{\text{th},E}$ (s)	ϵ_2^F	$T_{1/2}^{\text{th},F}$ (s)
^{54}Ti	1.5(4)	4280(160)	0.019	$30.5^{+7.3}_{-5.7}$	0.158	$10.2^{+2.3}_{-1.8}$
^{55}Ti	0.60(4)	7440(200)	0.019	$0.127^{+0.016}_{-0.013}$	0.158	$0.752^{+0.117}_{-0.099}$
^{56}Ti	0.15(3)	7030(330)	0.019	$0.515^{+0.138}_{-0.116}$	0.167	$0.465^{+0.136}_{-0.101}$
^{57}Ti	0.056(20)	11020(950)	-0.074	$0.0361^{+0.0216}_{-0.0127}$	0.167	$0.0420^{+0.0261}_{-0.0151}$

TABLE III. Decay characteristics of $^{54-56}$Ti: β-ray feeding intensity I_β for the level at excitation energy E in the daughter nucleus.

Isotope	I_β (%)	E (MeV)
^{54}Ti	90(20)	0.9(1)
^{55}Ti	60(10)	g.s.
	35(19)	1.0(2)
	5(3)	1.3(1)
^{56}Ti	$\sim$40	0.2–0.8

The distribution of the ^{57}Ti β-decay events indicates a small half-life [see Fig. 5(h)]. In this analysis the 330-ms half-life of the ^{57}V daughter decay [28] was taken into account. The result is the half-life $T_{1/2}^{\rm expt}=56$ (20) ms which is given in Table II.

B. Remeasurement of $^{58-60}$Cr

Within the limited statistics of the present experiment the half-life of ^{58}Cr was found to be in agreement with the more accurate previous result [30]. Spin values of the ^{58}Mn ground and isomeric states have recently been revised [31]. The 0^+ ground state in ^{58}Mn decays with a 3-s half-life. The decay measured in our experiments could be fitted with a 6-s parent, and 3-s daughter decay component.

For ^{59}Cr, decay curves were measured for β single events and $\beta\gamma$ coincidences. The result is the half-life 0.46 (5) s. In our analysis, the 4.6-s activity of ^{59}Mn [32] was neglected since it caused only a minor correction in the 1.6-s measuring interval. The present measurement of isotope-separated nuclei gives a higher accuracy than that obtained earlier from mass-separated samples [33]. For this isotope, 1239-keV and 112-keV γ rays with the relative intensities 1.00(11) and 0.08(2) have been reported [34]. Within the limited statistics and γ resolution of the present experiment one γ line at 1.2 MeV was clearly identified [see Fig. 6(a)].

In an earlier experiment on $A=60$ nuclei performed at the GSI mass separator half-lives of 0.57 (6) s and 51 (6) s were observed and assigned to ^{60}Cr and ^{60g}Mn, respectively [34]. As expected, in that multinucleon transfer reaction the production of the further-from-stability ^{60}Cr was by more than 1 order of magnitude smaller than that of ^{60}Mn [34]. In a later experiment investigating $A=60$ samples at the GSI mass separator doubly ionized ^{120}In nuclei were detected [31]. This gave cause to question the earlier assignment. In fact, if the earlier measured 51-s activity stems from the isomeric indium decay only, then the 0.57-s component would also have to be reassigned and it might belong to ^{60}Mn.

In the present measurement isotope separated ^{60}Cr was investigated and a β half-life of 0.51 (15) s was obtained. This result supports the earlier assignment of Ref. [34]; thus the long-lived ^{60g}Mn daughter activity can be neglected in the present half-life analysis. However, if the isomeric 3^+ state of ^{60m}Mn ($T_{1/2}=1.77$ s) is fed in 100% of the ^{60}Cr β decays a growth-and-decay analysis yields $T_{1/2}(^{60}\text{Cr})=0.47$ (15) s. This value is still in agreement with the earlier value 0.57 (6) s [33].

V. DISCUSSION

The results of these measurements can be compared to model considerations. If in ^{54}Ti decay the ^{54}V ground state is not directly fed (see Table III), this will be in the line of the adoption of a two-quasiparticle ^{54}V ground state, $\pi f_{7/2}\otimes\nu_{3/2}$. This configuration may only give rise to spin values $\geqslant 2^+$. In the β decay of ^{54}V the spin 3^+ was also indicated [24,25].

In the decay of ^{55}Ti our γ-ray data suggest a more complex decay. For the ^{55}V daughter, a ground-state spin in the interval $3/2^-\leqslant I^\pi\leqslant 7/2^-$ was discussed [25]. If for ^{55}Ti we adopt the spin $3/2^-$ as it is mainly found in the other odd-A $N=33$ isotones, a direct feeding of the ^{55}V ground state can be expected for ground-state spins $1/2^-$ to $5/2^-$. The ^{55}Ti decay which is followed by γ rays may feed excitation states in ^{55}V having similar spin values. Besides the observed $\beta\gamma$ coincidences, as given in Table III, unobserved branches cannot be excluded because of the very large ^{55}Ti-Q_β value.

A detailed structure calculation was then performed using the quasirandom-phase approximation (QRPA) model by Möller and Randrup [35] to calculate Gamow-Teller (GT) strength functions and β intensities and finally β-decay half-lives for the titanium isotopes. In this model, Folded-Yukawa wave functions and single-particle energies serve as the starting point to determine wave functions of the Ti parent ground states and V daughter ground states and excited states which are considered here. Pairing is treated in the Lipkin-Nogami approximation. Within these calculations it was only possible to use identical deformations for both parent and daughter nuclei. In order to demonstrate which of the levels may be involved in the GT decays of the $N\geqslant 32$ neutron-rich titanium isotopes, Fig. 7 gives the single-particle energies of ^{55}Ti as function of the nuclear deformation.

The nuclear ground-state deformations are calculated with recent microscopic-macroscopic mass models, namely the finite range droplet model (FRDM) [36], and the extended Thomas-Fermi with Strutinski-integral (ETFSI) model [37]. The results for the titanium isotopes obtained with the ETFSI model are the deformation values ϵ_2^E, and the values ϵ_2^F for the vanadium isotopes, obtained with the FRDM model. These disagreeing deformation values are given in Table II. They were then used in the QRPA calculations. The GT strength functions and β-ray intensities were derived by means of the experimental Q_β values [38]. Half-lives were calculated for both nuclear deformations ϵ_2^E and ϵ_2^F and are given in Table II. The errors of the half-life values correspond to the error margins of the experimental Q_β values only. The influence of first forbidden transitions could be neglected. This was checked by adding the strength from the gross theory [39] to the allowed strength which resulted in β half-lives which were by 2% smaller. In Table IV the calculated level characteristics, level energies and β feedings are given. In Fig. 8 the results of the β-ray transitions are shown obtained with the prolate deformation ϵ_2^F from the FRDM model. A compression of the abscissa into 0.25-MeV sections was done and the summed β strength of each interval is presented at the position of the central energy. As can

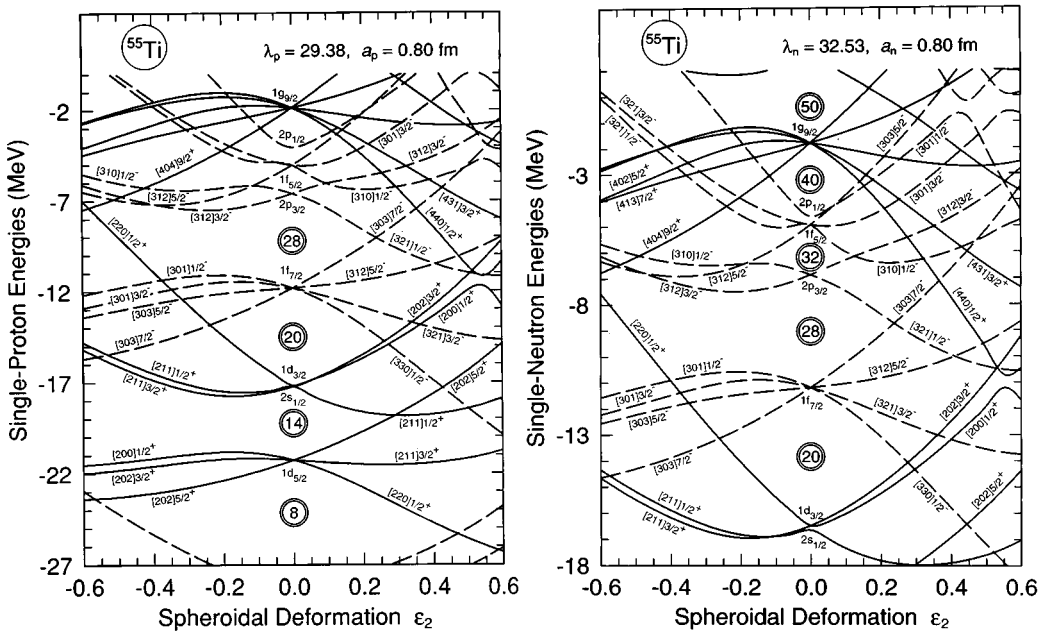

FIG. 7. Folded-Yukawa single-particle level schemes for ^{55}Ti protons and neutrons as a function of the deformation ϵ_2. The full lines correspond to orbitals with positive parity, the dashed lines to those with negative parity. Nilsson quantum numbers are given. Also indicated are the magic numbers for spherical and for finite deformations. The parameters λ_p and a_p, as well as λ_n and a_n, describe the depth and the shape diffuseness of the Folded-Yukawa potential.

be seen in Fig. 8, the expected decays are proceeding to low-lying daughter states.

For ^{55}Ti, we find an agreement between the experimental half-life and the value calculated with the FRDM model, while the half-lives calculated with the ETFSI model are too small. In the ^{55}Ti decay the feeding of one or two excited states is indicated (see Table III). The calculation gives low-lying one-quasiparticle (1QP) states (see Table IV and Fig. 8). These are low-spin states fed in allowed β decay branches. The measurement indicates intense ground-state–to–ground-state decay which is weakly indicated by the theory for prolate nuclei but rather reflected in the calculation for nearly spheroidal nuclei (Table IV). In ^{55}Ti β decay, two γ rays of 0.3 and 0.7 MeV with comparable intensity follow in cascade. Because we did not measure $\gamma\gamma$ coincidences, this should be verified.

The experimental half-life of ^{57}Ti agrees within limited accuracy with the calculation for slightly oblate and small prolate nuclear shapes (see Table II). The arbitrary assumption of a larger deformation would result in a longer theoretical half-life. The low counting statistics prevented the observation of γ rays in ^{57}Ti decay. According to the calcu-

TABLE IV. Calculated levels in V isotopes and their GT feedings according to the QRPA theory [35]. The QP configurations at excitation energy E are populated with intensities I_β relative to the number of titanium β decays. Only strong β branches are listed. The results are given for the values of deformation ϵ_2^E and ϵ_2^F, as listed in Table II.

Daughter isotope	ϵ_2^E			ϵ_2^F		
	QP config.	E^* (MeV)	I_β (%)	QP config.	E^* (MeV)	I_β (%)
^{54}V	π [330]1/2$^-$ $\otimes$ ν [301]1/2$^-$	1.05	28.4	π [321]3/2$^-$ $\otimes$ ν [310]1/2$^-$	0.14	15.3
	π [303]7/2$^-$ $\otimes$ ν [303]5/2$^-$	1.13	55.0	π [321]3/2$^-$ $\otimes$ ν [321]1/2$^-$	0.61	10.9
				π [312]5/2$^-$ $\otimes$ ν [312]3/2$^-$	0.77	39.2
^{55}V	π [330]1/2$^-$	g.s.	63.1	π [330]1/2$^-$	g.s.	3.9
	π [321]3/2$^-$	0.02	36.6	π [321]3/2$^-$	0.05	25.6
				π [312]5/2$^-$	0.60	65.7
^{56}V	π [330]1/2$^-$ $\otimes$ ν [301]1/2$^-$	0.68	31.4	π [321]3/2$^-$ $\otimes$ ν [310]1/2$^-$	0.23	10.0
	π [303]7/2$^-$ $\otimes$ ν [303]5/2$^-$	0.75	62.6	π [321]3/2$^-$ $\otimes$ ν [301]3/2$^-$	0.40	15.6
				π [312]5/2$^-$ $\otimes$ ν [301]3/2$^-$	0.77	24.6
				π [321]3/2$^-$ $\otimes$ ν [321]1/2$^-$	1.34	29.6
^{57}V	π [301]3/2$^-$	0.30	29.6	π [330]1/2$^-$	g.s.	3.9
	π [301]1/2$^-$	0.40	57.8	π [321]3/2$^-$	0.40	21.7
				π [312]5/2$^-$	0.48	58.8

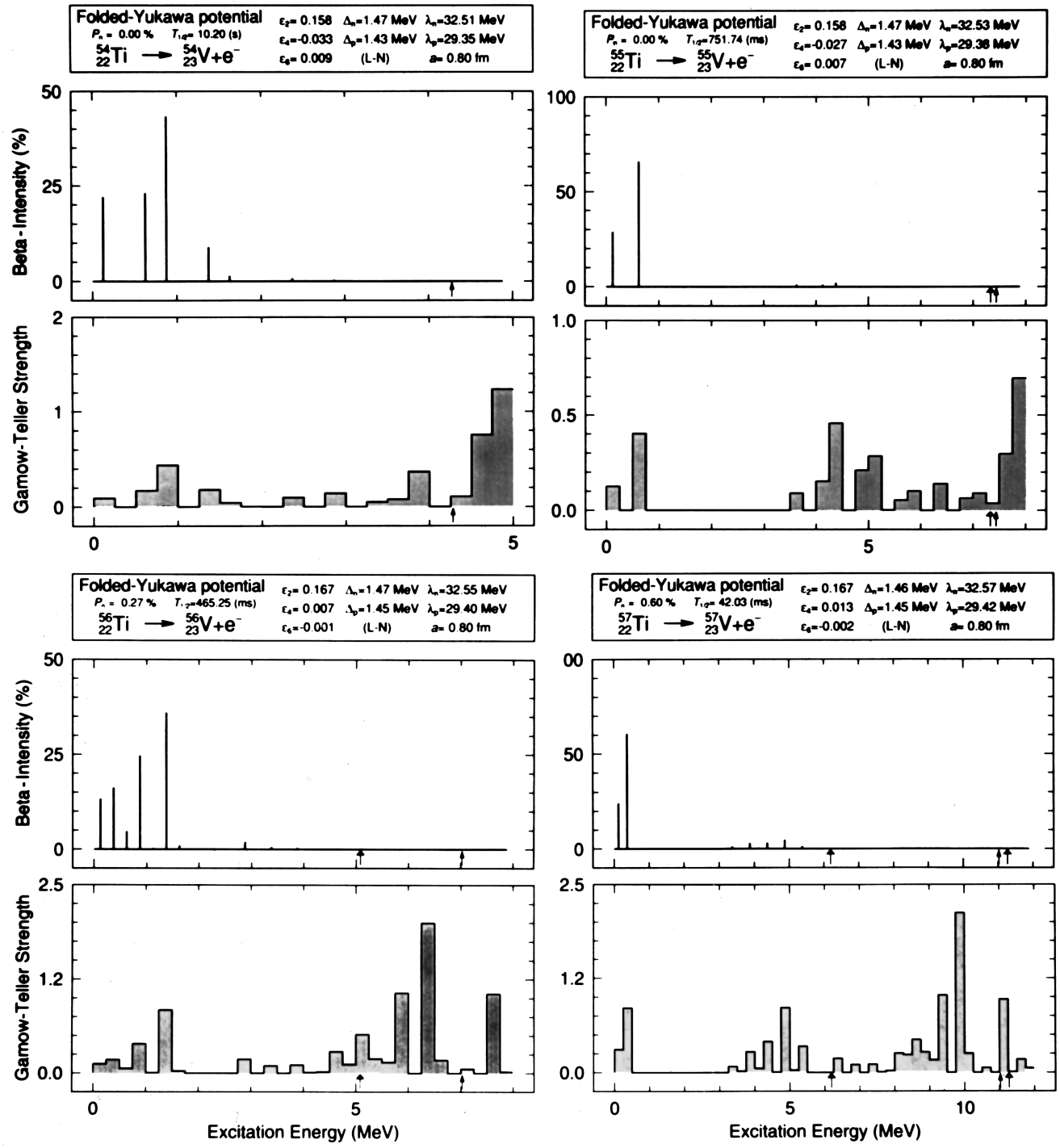

FIG. 8. Calculated Gamow-Teller strength functions and β intensities as function of the excitation energy for ^{54}Ti (left top), ^{55}Ti (right top), ^{56}Ti (left bottom), and ^{57}Ti (right bottom). The deformation parameters ϵ_2^F are used (see Table II). The strength is summed in 0.25-MeV intervals (see text).

lation the situation should be similar to the one in ^{55}Ti decay. A reinvestigation of ^{57}Ti would also be of interest because the calculation gives a small branching of β-delayed neutron emission of $P_n \sim 0.6\%$ for the deformation ϵ_2^F.

In ^{54,56}Ti decays the experimental half-lives cannot be reproduced by the calculation with ϵ_2^E or ϵ_2^F deformations. In fact, the small experimental half-life of ^{54}Ti corresponds to a logft value <4, while the calculated decay branches have log$ft \sim 5$. The energies of 2QP states were calculated and the β feeding of these configurations were derived as given in Table IV. In addition, for both isotopes and prolate deformations ϵ_2^F the expected β feeding of the ground states is much less than 1%, which is in agreement with the experiment (see above). The experimental 0.9-MeV γ ray of ^{54}Ti and some γ-ray intensity at lower energy [see Table III and Fig. 6(b)] might be correlated with γ transitions of such 2QP states as given in Table IV. The same holds for the γ rays of ^{56}Ti.

In the ^{56}Ti decay β transitions to the ^{56}V excited states

are experimentally indicated (see Table III). The calculations for both values of deformation do not exhibit any β transition to the ^{56}V ground state.

For calcium and chromium isotopes a sudden decrease in the β-ray half-lives was observed when the $N=32$ shell was surpassed [5–8]. Such an $N=32$ subshell effect may also be indicated by the result of our QRPA calculation. In ^{54}Ti, the highest occupied state is the $\nu 2p_{3/2}$ shell, and the β strength originating from a $\nu f_{5/2}$ contribution might be small (see Fig. 7). For ^{55,56}Ti at prolate deformation, however, low-Ω states of the $\nu f_{5/2}$ shell are occupied, resulting in strong GT transitions between $\pi f_{7/2}$ and $\nu f_{5/2}$ configurations. Such a shell effect was not observed in our experiment.

In order to clarify further this situation, better statistics measurements as well as QRPA calculations which can take into account a change of the nuclear shape between parent and daughter nucleus are required.

ACKNOWLEDGMENTS

We would like to thank the technical collaborators of LISE3/GANIL for their assistance before and during the experiment. This work was supported by the German Ministry of Research and Technology (BMFT) under Contract No. 06GÖ667/TP3, and by the Deutsche Forschungsgemeinschaft (DFG) under Contract No. Kr806/3. We would like to acknowledge support from the European Community under Contract No. ERBCHGE-CT94-0056 (Human Capital and Mobility, Access to the GANIL large scale facility). One of us (T.R.) would like to thank the A. v. Humboldt Stiftung for financial support.

[1] D. Guillemaud-Mueller, Y. E. Penionzhkevich, R. Anne, A. C. Artukh, D. Bazin, V. Borrel, C. Détraz, D. Guerreau, B. V. Gvozev, J. C. Jacmart, X. Jiang, A. M. Kalinin, V. V. Kamanin, V. B. Kutner, M. Lewitowicz, S. M. Lukyanov, A. C. Mueller, N. Hoai Chau, F. Pougheon, A. Richard, M. G. Saint-Laurent, and W.-D. Schmidt-Ott, Z. Phys. A **332**, 189 (1989).

[2] A. C. Mueller and B. M. Sherill, Annu. Rev. Nucl. Part. Sci. **43**, 529 (1993).

[3] T. R. Werner, J. A. Sheikh, W. Nazarewicz, M. R. Strayer, U. S. Umer, and M. Misu, Phys. Lett. B **333**, 303 (1994).

[4] W. Böhmer, K.-L. Kratz, P. Möller, and B. Pfeiffer, Verh. Dtsch. Phys. Ges. (VI) **30**, 588 (1995); W. Böhmer, Ph.D. thesis, University of Mainz, Germany, 1996 (unpublished).

[5] A. Huck, G. Klotz, A. Knipper, C. Miehe, C. Richard-Serre, G. Walter, A. Poves, H. L. Ravn, and G. Marguier, Phys. Rev. C **31**, 2226 (1985).

[6] M. Langevin, C. Detraz, D. Mueller-Guillemaud, A. C. Mueller, C. Thibault, G. Klotz, C. Miehe, G. Walter, M. Epherre, and C. Richard-Serre, Phys. Lett. **130B**, 251 (1983).

[7] B. J. Dropesky, A. W. Schardt, and T. T. Shull, Nucl. Phys. **24**, 357 (1960).

[8] C. N. Davids, D. F. Geesaman, S. C. Tabor, M. J. Murphy, E. B. Norman, and R. C. Pardo, Phys. Rev. C **17**, 1815 (1978).

[9] O. Sorlin, D. Guillemaud-Mueller, A. C. Mueller, V. Borrel, S. Dogny, F. Pougheon, K.-L. Kratz, H. Gabelmann, B. Pfeiffer, A. Wöhr, W. Ziegert, Y. E. Penionzhkevich, S. M. Lukyanov, V. S. Salamantin, R. Anne, C. Borcea, L. K. Fifield, M. Lewitowicz, M. G. Saint-Laurent, D. Bazin, C. Détraz, F.-K. Thielemann, and W. Hillebrandt, Phys. Rev. C **47**, 2941 (1993).

[10] C. L. Harper, *Nuclei in the Cosmos III* (IOP, London, 1993), p. 113.

[11] D. G. Sandler, S. E. Koonin, and W. A. Fowler, Astrophys. J. **259**, 908 (1982).

[12] M. Harris, Astrophys. J. **264**, 613 (1982).

[13] W. Ziegert, M. Wiescher, K.-L. Kratz, P. Möller, J. Krumlinde, F.-K. Thielemann, and W. Hillebrandt, Phys. Rev. Lett. **55**, 39 (1985).

[14] D. Hartmann, S. E. Woosley, and M. F. El Eid, Astrophys. J. **297**, 837 (1985).

[15] W. Hillebrandt, K.-L. Kratz, F.-K. Thielemann, and W. Ziegert, in *Weak and Electromagnetic Interactions in Nuclei*, edited by H. V. Klapdor (Springer-Verlag, Berlin, 1986), p. 987.

[16] R. Anne, D. Bazin, A. C. Mueller, J. C. Jacmart, and M. Langevin, Nucl. Instrum. Methods A **257**, 215 (1987).

[17] R. Anne and A. C. Mueller, Nucl. Instrum. Methods B **70**, 276 (1992).

[18] U. Bosch-Wicke, W.-D. Schmidt-Ott, K. Rykaczewski, T. Hild, K. Becker, H. Keller, R. Kirchner, O. Klepper, V. Kunze, F. Meissner, A. Piechaczek, E. Roeckl, and D. Schardt, in *Proceedings of the Sixth International Conference on Nuclei Far From Stability and the Ninth International Conference on Atomic Masses and Fundamental Constants*, Bernkastel-Kues, Germany, 1992, Inst. of Phys. Conf. Ser. No. 132, edited by R. Neugart and A. Wöhr (IOP, London, 1993), p. 723.

[19] H. Keller, R. Kirchner, O. Klepper, E. Roeckl, D. Schardt, R. S. Simon, P. Kleinheinz, C. F. Liang, and P. Paris, Nucl. Instrum. Methods A **300**, 67 (1991).

[20] K. Becker, Diploma thesis, Universität Göttingen, Germany, 1988 (unpublished).

[21] X. -L. Tu, X. G. Zhou, D. J. Vieira, J. M. Wouters, Z. Y. Zhou, H. L. Seifert, and V. G. Lind, Z. Phys. A **337**, 361 (1990).

[22] H. L. Seifert, J. M. Wouters, D. J. Vieira, H. Wollnik, X. G. Zhou, X. L. Tu, Z. Y. Zhou, and G. W. Butler, Z. Phys. A **349**, 25 (1994).

[23] W. K. Press, S. A. Peukolsky, W. T. Vetterling, and B. P. Flannery, *Numerical Recipes in C – The Art of Scientific Computing*, 2nd ed. (Cambridge University Press, Cambridge, England, 1992), p. 683.

[24] T. E. Ward, P. H. Pile, and P. K. Kuroda, Nucl. Phys. **A148**, 225 (1970).

[25] E. K. Warburton, J. W. Olness, A. M. Nathan, and A. R. Poletti, Phys. Rev. C **18**, 1637 (1978).

[26] A. M. Nathan, D. E. Alburger, J. W. Olness, and E. K. Warburton, Phys. Rev. C **16**, 1566 (1977).

[27] F. Ameil, P. Armbruster, M. Bernas, S. Czajkowski, Ph. Dessagne, C. Donzaud, H. Geissel, A. Grewe, E. Hanelt, A. Heinz, Z. Janas, M. de Jong, C. Kozhuharow, C. Miehe, W. Schwab, and S. Steinhäuser, in *Proceedings of ENAM 1995* Arles,

France, 1995, edited by M. de Saint-Simon and O. Sorlin (Edition frontière, Singapore, 1995), p. 537.

[28] O. Sorlin, T. Dörfler, R. Anne, W. Böhmer, V. Borrel, D. Guillemaud-Mueller, S. Grévy, K.-L. Kratz, M. Lewitowicz, T. Mehren, A. C. Mueller, A. Ostrowsky, F. Pougheon, I. Rabout, T. Rauscher, M. Robinson, M. G. Saint-Laurent, and W.-D. Schmidt-Ott, in *Proceedings of ENAM 1995* [27], p. 603.

[29] Thomas Dörfler, Ph.D. thesis, Universität of Göttingen, Germany, 1996 (unpublished); O. Sorlin, V. Borrel, S. Grévy, D. Guillemaud-Mueller, A. C. Mueller, F. Pougheon, I. Rabout, W. Böhmer, K.-L. Kratz, B. Pfeiffer, T. Mehren, T. Rauscher, M. G. Saint-Laurent, M. Lewitowicz, R. Anne, A. Ostrowski, M. Robinson, T. Dörfler, and W.-D. Schmidt-Ott (unpublished).

[30] T. E. Ward, P. H. Pile, and P. K. Kuroda, Phys. Rev. **182**, 1186 (1968).

[31] W.-D. Schmidt-Ott, K. Becker, U. Bosch-Wicke, T. Hild, F. Meissner, R. Kirchner, E. Roeckl, and K. Rykaczewski, in [18], p. 627.

[32] R. C. Pardo, C. N. Davids, M. J. Murphy, E. B. Norman, and L. A. Parks, Phys. Rev. C **16**, 370 (1977).

[33] U. Bosch, W.-D. Schmidt-Ott, P. Tidemand-Petersson, E. Runte, W. Hillebrandt, M. Lechle, F.-K. Thielemann, R. Kirchner, O. Klepper, E. Roeckl, K. Rykaczewski, D. Schardt, N. Kaffrell, M. Bernas, P. Dessagne, and W. Kurcewicz, Phys. Lett. **164B**, (1985).

[34] U. Bosch, W.-D. Schmidt-Ott, E. Runte, P. Tidemand-Petersson, P. Koschel, F. Meissner, R. Kirchner, O. Klepper, E. Roeckl, K. Rykaczewski, and D. Schardt, Nucl. Phys. **A477**, 89 (1988).

[35] P. Möller and J. Randrup, Nucl. Phys. **A514**, 1 (1990).

[36] P. Möller, M. D. Myers, J. R. Nix, and W. J. Swiatecki, At. Data Nucl. Data Tables **59**, 185 (1995).

[37] Y. Aboussir, J. M. Pearson, A. K. Dutta, and F. Tondeur, At. Data Nucl. Data Tables **61**, 127 (1995).

[38] G. Audi and A. H. Wapstra, Nucl. Phys. **A565**, 1 (1993).

[39] K. Takahashi, M. Yamada, and T. Kondoh, At. Data Nucl. Data Tables **12**, 101 (1973).